J Chem Biol (2014) 7:43–55
DOI 10.1007/s12154-013-0104-7

ORIGINAL ARTICLE

Quantification of exocytosis kinetics by DIC image analysis of cortical lawns

James Mooney · Saumitra Thakur · Peter Kahng · Josef G. Trapani · Dominic Poccia

Received: 17 June 2013 / Accepted: 1 September 2013 / Published online: 27 September 2013

Abstract Cortical lawns prepared from sea urchin eggs have offered a robust in vitro system for study of regulated exocytosis and membrane fusion events since their introduction by Vacquier almost 40 years ago (Vacquier in Dev Biol 43:62–74, 1975). Lawns have been imaged by phase contrast, darkfield, differential interference contrast, and electron microscopy. Quantification of exocytosis kinetics has been achieved primarily by light scattering assays. We present simple differential interference contrast image analysis procedures for quantifying the kinetics and extent of exocytosis in cortical lawns using an open vessel that allows rapid solvent equilibration and modification. These preparations maintain the architecture of the original cortices, allow for cytological and immunocytochemical analyses, and permit quantification of variation within and between lawns. When combined, these methods can shed light on factors controlling the rate of secretion in a spatially relevant cellular context. We additionally provide a subroutine for IGOR Pro® that converts raw data from line scans of cortical lawns into kinetic profiles of exocytosis. Rapid image acquisition reveals spatial variations in time of initiation of individual granule fusion events with the plasma membrane not previously reported.

Keywords Exocytosis · DIC · Cortical granules · Sea urchin · Membrane fusion

P. Kahng · J. G. Trapani · D. Poccia (✉)
Department of Biology, Amherst College, Amherst, MA 01002, USA
e-mail: dlpoccia@amherst.edu

J. Mooney · S. Thakur · J. G. Trapani · D. Poccia
Program in Neuroscience, Amherst College, Amherst, MA 01002, USA

Introduction

Exocytosis is achieved by heterotypic fusion of secretory vesicles with plasma membranes resulting in delivery of vesicle contents to the extracellular space. Among the most studied systems of exocytosis is the secretion of neurotransmitters by neurons. Neurosecretion is an enormously complex process in vivo involving overlapping phases of transport, priming, docking, fusion, and endocytic reuptake events [18, 27]. Additionally, in vitro systems from neuroendocrine cells or neurons require ill-defined cytosol for exocytosis [1, 23]. A simpler and better-defined in vitro system has been developed for the study of secretion from sea urchin oocytes [24].

Exocytosis of sea urchin egg secretory vesicles (cortical granules (CGs) or cortical vesicles) occurs in vivo in response to a wave of Ca^{++} release that spreads across the egg cortex once initiated from the point of sperm entry at fertilization [14]. Cortical granules are typical of animal eggs that undergo holoblastic cleavage. They possess many advantages for studies of exocytosis. The granules are considerably larger than neurosecretory vesicles. An in vitro system is simple to prepare and does not require priming, docking, or cytosolic factors, does not undergo endocytosis, and remains stable and responsive for many hours [24].

Originally, the system was prepared by adhering dejellied eggs to protamine sulfate-coated glass surfaces and shearing them with jets of Ca^{++}-free seawater, thus washing away endoplasmic structures and non-adherent portions of the cell cortex. The resulting cortical "lawns" consist of circular pieces of vitelline layer–plasma membrane approximately the diameter of the egg to which densely packed cortical granules are attached on the cytoplasmic face. Observed by scanning electron microscopy, the granules have struts that appear to attach them to the plasma membrane and are interspersed with uncharacterized ~0.5 μm diameter vesicles [24]. In addition, variable amounts of endoplasmic reticulum (ER) may remain attached [20–22].

Initial observations of in vitro exocytosis in this system were made by light microscopy. The "planar" or lawn in vitro system is sometimes replaced by suspensions of isolated fragments of cortices (cell surface complexes or CSCs) in which exocytosis is measured by light scattering techniques. These are prepared by gentle homogenization of eggs and centrifugal purification of the resulting cortices with CGs firmly attached to plasma membrane fragments. However, CSCs fold over and are not ideal for microscopy. In both planar and CSC assays, cortical granule membranes fuse with the plasma membrane as they do in vivo.

Exogenously added Ca^{++} triggers granule discharge at near physiological concentrations. In the absence of the Ca^{++} chelator EGTA, initiation of exocytosis in lawns can occur either spontaneously or by mechanical disruption in a wave spreading from the point of injury. The latter has been speculated to arise from endogenous Ca^{++} originating within the CGs themselves [15, 24]. Other potential sources of free Ca^{++} such as ER fragments and smaller vesicles are usually ignored in kinetic analyses of lawns or CSCs.

Isolated CGs can be prepared by dissociation from CSCs upon treatment at pH 9.1 and differential centrifugation. Much valuable quantitative data on cortical granule fusion has been derived from the cortical granule-cortical granule (CG-CG) fusion in such preparations [7]. However, it should be noted that this homotypic fusion does not occur in the egg in vivo, and preparation of the system destroys the normal spatial relationship of CGs and plasma membrane and perhaps other cortical components which could modulate responses. Isolated CGs can also fuse with liposomes in vitro. CG-CG fusion is typically monitored by light scatter which yields averaged data from large numbers of granules derived from many thousands of eggs.

Many elegant experiments using CG-CG fusion have led to mechanistic insights into the fusion process, including Ca^{++} sensitivity determinations, cholesterol dependence, and estimations of minimal fusion machinery requirements [2, 4, 6, 16, 25, 29]. However, since neither CG-CG fusion nor CG-liposome fusion occurs in vivo, the data must be cautiously interpreted. This is particularly true because protein and lipid compositions of the plasma membrane and cortical granule membranes are far from identical [9, 10, 12, 13]. However, quantitative assays on adherent lawns or suspensions of CSCs are more difficult to obtain experimentally, requiring special flow cells and light scattering microscopy techniques. They are not generally high throughput assays and show more variability than CG-CG assays.

We sought to develop a simple, inexpensive, and quantitative assay for cortical granule/plasma membrane fusion in cortical lawns that would retain the original spatial relationships of the two partners and avoid extreme conditions of preparation. The preparation would also allow for simultaneous monitoring by microscopy of intermediate extents of exocytosis to better distinguish fusion events without assuming average properties of the system. We wanted to compare variation between individual lawns in a population, and to be able eventually to combine analyses with cytological evaluations including immunocytochemical analyses. Using analysis of differential interference contrast images of cortical lawns in combination with inexpensive disposable reaction vessels, we generated kinetic curves comparable to those published, but which reveal spatial heterogeneities in the response to Ca^{++} not previously appreciated. By preserving the original architecture of the secretory system, these techniques appear to permit more detailed investigations into the roles of various cortical elements in exocytosis.

Materials and methods

Construction of disposable reaction vessels Circular holes (0.7" (18 mm)) were cut in the center of 60×15 mm polystyrene Petri dishes (Falcon 351007) with a hole saw and the bottom surface deburred to allow close adherence of coverslips. A set of short tubes (0.5" (13 mm) long) was cut from a piece of cast acrylic tubing (1" (25 mm) o.d., 0.75" (19 mm) i.d.) from US Plastics, Lima, OH. Each tube was attached to a Petri dish with methylene chloride acrylic adhesive (Caseway SC-125, McMaster-Carr, Elmhurst, Illinois) as shown in Fig. 1. A 22× 22 mm no. 1 coverslip was sealed to the bottom of each dish using stopcock grease and secured with nail polish. The cylindrical chamber, thus formed, has a capacity of ~3 ml. A larger coverslip may be used for better adherence and the height of the tube increased if more mixing capacity is desired.

Rates of equilibration of exogenously added solutions in the chambers were estimated in two ways. Using a fluorescein isothiocyanate (FITC) filter set, a time series reading of baseline intensity was acquired in line-scan mode on a Zeiss Pascal confocal microscope. Images were acquired at the focal plane of the coverslip surface during dilution of 1 ml of baseline intracellular medium (BIM) buffer (210 mM potassium glutamate, 500 mM glycine, 10 mM NaCl, 10 mM PIPES, 50 mM $CaCl_2$, 1 mM$MgCl_2$, 1 mM EGTA, pH 6.7) [5, 6] containing 2 mM FITC and 10 % Mowiol–DABCO antifade by using an equal volume of this solution lacking FITC. Alternatively, a thin fluorescent protein layer was prepared from egg white protein labeled with FITC in carbonate buffer, pH 9.5 [11] to yield a fluorescent, denatured protein adhering firmly to the coverslip that is sensitive to pH changes. Gain or loss of FITC fluorescence intensity at the level of the coverslip was measured as above, either by initially equilibrating the protein at pH 8 and diluting it to pH 4 with addition of citrate buffer, or equilibrating at pH 4 and diluting to pH 8 with carbonate buffer.

Reagents and preparation of lawns Cover slips were cleaned with Alconox detergent in hot water and rinsed thoroughly

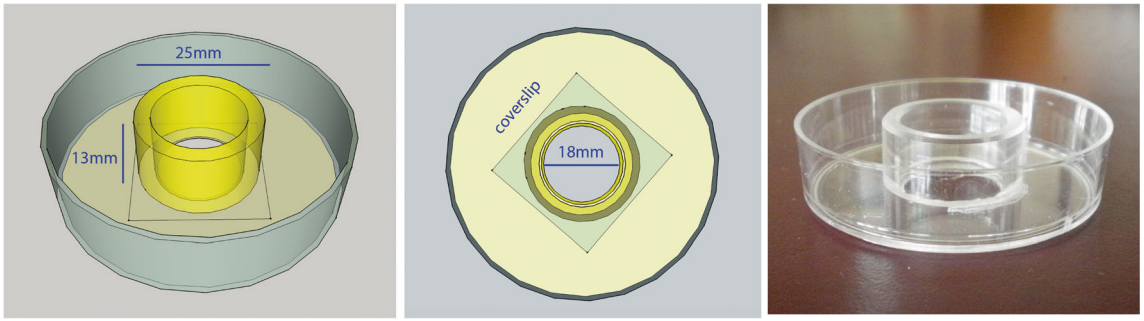

Fig. 1 Schematic diagrams and photograph of a disposable reaction vessel used to monitor exocytosis by DIC optics. An acrylic cylinder is attached to the inside of a Petri dish into which a circular hole had been cut. A coverslip coated with protamine sulfate is attached to the outside of the dish with vacuum grease and nail polish. Cortical lawns are prepared inside the assembly which is subsequently mounted on an inverted microscope

with distilled water. Cover slips were coated with 1 % (w/v) protamine sulfate (Sigma-Aldrich) for 10 min before rinsing thoroughly with distilled water and drying. Sea urchin eggs were dejellied by washing twice with Ca^{++}-free 0.22 μm Millipore-filtered seawater (MFSW), 0.1 M citric acid, and pH 5 for 1 min each, washed three times in normal MFSW, pH8, and then resuspended in BIM. Lawns were prepared in the assembled chambers by adding ~80 μl of concentrated egg suspension onto the surface of the coated coverslip, and allowing eggs to adhere for 20 min while the top of the chamber was covered with an untreated coverslip to prevent evaporation. The adherent eggs were subsequently sheared with a jet of BIM from a fine tip plastic Pasteur pipette held at 45° and moved back and forth in a Z-pattern. Lawns were promptly evaluated on an inverted phase contrast microscope for extent and uniformity of shearing, re-sheared if necessary, and stored under 1 ml of BIM until reacted.

Appropriate samples were placed under differential interference microscopy (DIC) optics on a confocal microscope. Typically, exocytosis was initiated by rapid addition from a 5 ml glass pipette of 1 ml of a 2X $CaCl_2$ in BIM solution to the 1 ml of BIM covering the lawns in the chamber. This results in fast equilibration with minimal but sufficient disturbance of the surface. Optical disturbance serves as an indicator of the time of solution application in the DIC images. Free Ca^{++} final concentrations were calculated for each run from the final concentrations of buffer components after mixing using the Ca-EGTA Calculator v1.3 available at http://www.stanford.edu/~cpatton/CaEGTA-TS.htm.

Microscopy DIC image data were taken on either a Zeiss LSM5 Pascal or a Nikon Eclipse Ti confocal microscope using the 488 nm line of the argon laser as light source. In principle, any DIC equipped microscope with a fast digital camera can be used, since the DIC images are not confocal. DIC optics were adjusted visually before beginning experiments using either a 40X objective to provide finer details of individual lawns or a 20X objective for accumulation of images from larger numbers of lawns (typically ~50/field). For kinetic analyses, either line scans or images of the field were used. In either case, the standard deviation of image pixel intensities about the mean value of background intensity were used to generate exocytosis kinetic curves (kinetic data), as the intensities of the black and white edges of each granule converge towards an intermediate gray endpoint. For Ca^{++} titration curves (endpoint data), images were collected from a 3×3 grid pattern of nine fields in the Nikon confocal using its motorized stage.

Line scan data analysis Pixel intensity data from a time-series of line scans were output to a Zeiss LSM-format file. Data were collected at a 10 Hz sample rate for a minimum of 40 s following calcium addition. Since Zeiss Pascal software does not allow parsing of the time series from these files, the data file was imported into IGOR Pro software (WaveMetrics) using the import program LSM Reader by Stephen R. Ikeda (http://www.igorexchange.com/project/LSMreader). A typical line scan recorded intensities across a field of 350–450 μm in length encompassing four cortical lawns from a 5 megapixel image field. Gain, offset, and shear were adjusted on the microscope to optimize the intensity difference across each cortical granule. The background intensity was set at 100 units for each run.

In order to analyze the time-course of the changes in pixel intensity following Ca^{++}-evoked secretory events, we wrote a subroutine called Line Scan Analysis within Igor Pro (available online on IGOR Exchange http://www.igorexchange.com/project/LS_analysis). The subroutine analyzes the raw pixel intensity from a time-series of line scans, each of which appears both as a series of peaks and troughs of intensities as the scan moves across each granule within a lawn, and as a stretch of static intensity as the scan moves in between lawns. Across a time-series of line scans, the addition of Ca^{2+} and subsequent granule fusion causes the within-lawn peaks and troughs to converge towards the mean background pixel intensity as CGs fuse with the plasma membrane. Initially, the subroutine presents a single line scan for the user to identify each lawn by setting pairs of cursors at their borders. The subroutine then analyzes only the line-scan data within each pair of cursors (i.e., the within-lawn pixel intensities). For each time point (i.e., line scan), the standard deviation (or other user-chosen statistic) is

determined from the cumulative intensities from all the within-lawn pixels. The procedure is invoked from the macro Line Scan Analysis, and the user is presented with a panel to choose a statistic and other options. The user can also manually enter a sampling rate (i.e., the inter line-scan interval) for proper graphic display of the data, can choose whether to baseline the data (to correct for drift), and has the option to output a graph with a curve fit of the analyzed data. In addition, the panel has an option to analyze LSM data imported with the LSM reader (such as the output from the Zeiss confocal), or as a tiff file of line scan data (as output from the Nikon confocal), and the subroutine can be adapted for other formats.

Two-dimensional image analysis Image file time sequences were obtained in either Zeiss (.lsm) or Nikon (.nd2) file formats with confocal microscopes. Typically, 256×256 pixel images using a 20X objective were taken every 294 ms. Therefore, the assay records the intensity of over 65,000 pixels in a field of view, with up to ¾ of them contributed by the lawns.

For kinetic data, images were imported into Volocity 6.0 software (Improvision, PerkinElmer). In principle, any image analysis package that can measure image intensities within regions of interest (ROIs) can be substituted, such as the free open-source program ImageJ from NIH http://rsb.info.nih.gov/ij/. ROIs were defined as indicated in the Results section either as one or more circular lawns or a nested set of circular concentric ROIs constructed for a given lawn. The intensity values for each time point within an ROI are obtained from the Volocity *Measurements* menu, using *Threshold>Find Objects* in *ROI>Measure>Intensity*, resulting in a spreadsheet of values indexed by time point. Data from multiple lawns can be merged together to a single ROI by selecting all lawn ROI's using the *Edit>ROI>Merge* function. Kinetic curves are generated from the values relative time (s) and standard deviation of intensity, which are exported from Volocity to IGOR Pro to construct fitted decay curves.

For Ca^{++} sensitivity endpoint assays, two-dimensional data were collected from nine fields each containing ~50 lawns (~100,000 granules in total) using a 20X objective. Measurements of standard deviation were made after importing images into Volocity. This was accomplished using the *Find Objects in ROI* tool found under the *Measurements* menu. The ROI was selected as the entire image with lawns typically constituting ~75 % of the image field area. Measurements of standard deviation for this ROI were then copied into Microsoft Excel and grouped with the corresponding standard deviations for the following experimental conditions: before calcium, after calcium, and after excess calcium for each stage position. To ensure full exocytosis, excess free [Ca^{++}] was set to 10 mM. Percent exocytosis for each intermediate free [Ca^{++}] was calculated from the value (after)/((before) − (after excess)). Calcium sensitivity curves (percent exocytosis vs. log free [Ca^{++}]) were fit to a sigmoidal function in Igor Pro.

Results

Reaction vessel and mixing conditions

We first devised an inexpensive reaction vessel that would be compatible with various types of light microscopy and would permit rapid equilibration of exogenously introduced solutions (Fig. 1). Its construction is described in Materials and methods. Lawns were prepared after adherence of eggs to a protamine sulfate-coated coverslip that forms the bottom of the chamber. To test for rapidity and completion of solution mixing, the assembly was placed onto the stage of an inverted microscope and the focus adjusted to the level of the coverslip. Mixing was monitored by including FITC in 1 ml of BIM buffer in the chamber and rapidly diluting it with 1 ml of buffer not containing FITC, while measuring the decline in fluorescence with the line scan function of the confocal microscope. As seen in Fig. 2a, the fluorescence signal quickly declined during the initial 10 ms and was stable by ~150 ms after dilution. A second assay devised by Kaplan et al. [11] measures a response at the level of the coverslip to a buffer pH change detected by the pH-dependent fluorescence intensity of a thin layer of FITC-egg white protein deposited on the coverslip. The protein was adjusted to pH 8 in carbonate buffer and shifted to buffer pH 4 with citrate buffer for vice versa. In both cases, pH equilibrated within ~400 ms (Fig. 2b, c).

Use of DIC optics

When cortical granules are imaged with DIC, the border of each granule is of a high contrast compared to within and outside the granule. Following exocytosis, this highly contrasted periphery disappears from each granule. Figure 3a and b show fields of intact lawns. Upon addition of exogenous Ca^{++} (Fig. 3c, d), the contrast across granules decreased to background as granules fused with the underlying plasma membrane leaving "domes" of granule membranes continuous with the plasma membrane following mixing of the contents of the vesicles with the buffer between the plasma membrane and vitelline layer adherent to the coverslip [29]. We took advantage of this decrease in contrast as each granule fuses with the plasma membrane as a quantitative measure of exocytosis.

DIC is very sensitive to inhomogeneities (stress) in the optical pathway. In our system, only one coverslip is present. Transient image perturbation upon addition of the second solution serves as a zero time marker that occurs at variable times before the cortical granule response is initiated. This time is sufficient, however, for solution equilibration to occur prior to the response. Focus is maintained by strong attachment of the coverslip to the plastic dish by vacuum grease and nail polish with sufficient overlap of the adherent regions to resist bending in the middle of the coverslip.

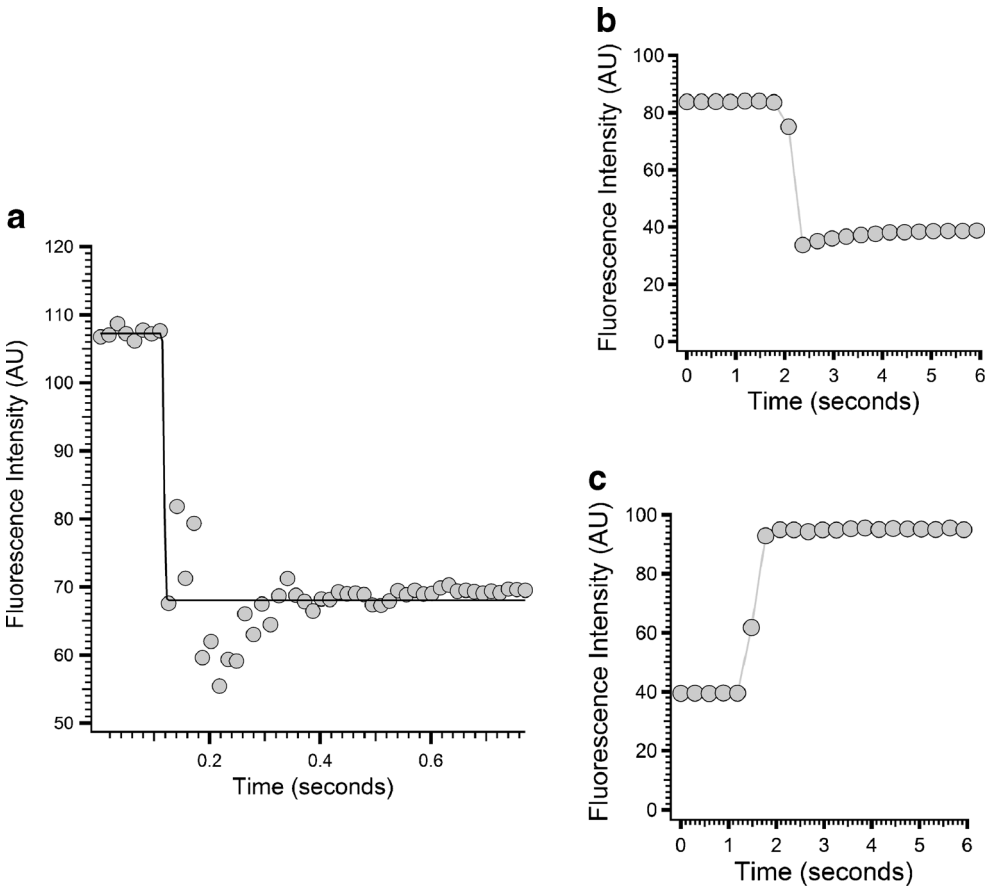

Fig. 2 Rate of equilibration of exogenously added solutions at the level of the vessel cover slip. **a** Loss of FITC fluorescence at the bottom of the chamber upon addition of an equal volume of buffer lacking FITC. **b** Change in fluorescence intensity of a thin FITC-egg white layer on the coverslip upon alteration of pH by an equal volume of added solution from pH 4 to 8 or **c** pH 8 to 4

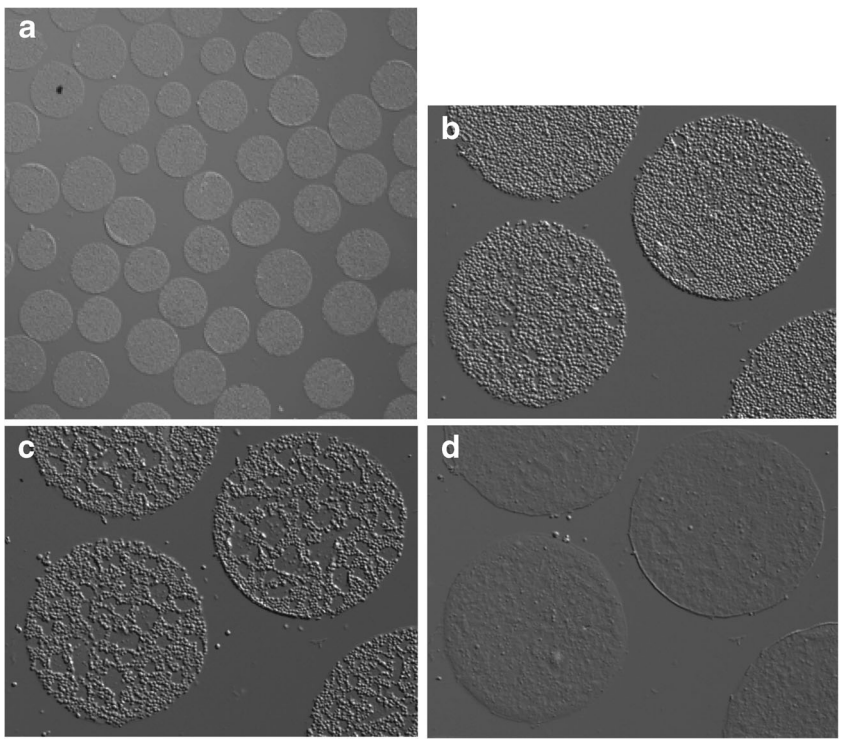

Fig. 3 Endpoint assay of exocytosis. **a** A field of ~50 whole lawns viewed under a 20X objective. Differential interference contrast images of the same region of the field taken before (**b**) and after (**c**) addition of 20 μM free Ca^{++}. **d** After further addition of 10 mM Ca^{++} to yield complete exocytosis

Line scan assay of exocytosis

Line scans of image intensity were used to rapidly acquire kinetic data for decay curves from the loss of contrast occurring at the edges of granules as exocytosis occurs. The decrease in contrast was measured as the standard deviation of pixel intensities versus the average background pixel intensities to which they converge. The background is not zero because of the small amount of contrast caused by the residual domes. The absolute values of standard deviations depend on adjustment of the settings for the average background contrast. Scans can be taken in as briefly as 1-ms intervals. Using the software of a Zeiss Pascal confocal microscope, a line is drawn across several lawns in the direction of the shear axis (indicated by the maximal intensities of light and dark regions or "shadow-casts" surrounding each granule). Scanning through the center of each spherical object like a cortical granule results in a peak and trough corresponding to the bright and dark edges of the object. Plotted as intensity, such a line corresponds to the first derivative of the optical path difference curve (http://micro.magnet.fsu.edu/primer/techniques/dic/dicintro.html), which produces regions of higher and lower amplitude and, therefore, contrast. Generally, scans taken every 100 ms are sufficient to generate composite decay curves lasting 5–10 s, but much shorter sampling intervals are possible. Although individual traces of these data can be displayed by the LSM Pascal software, there is no included export function that conveniently allows for further data analysis. We, therefore, used an LSM import program to read the data into Igor Pro and wrote a subroutine to convert the raw data to decay curves.

An example of the raw data in the form of a series of peaks and troughs, each pair representing a scan across an intersected granule, is shown in Fig. 4. The red arrow in Fig. 4a indicates the placement of the scan line. The brightest and weakest intensity peaks decay towards background with time (traces before and after complete exocytosis uncorrected for background are shown in Fig. 4b). Variation in background in this case is due to positioning of the Wollaston prisms, and, normally, this is adjusted to be much more uniform across the field of view. The time series of such data are analyzed by our subroutine, which corrects the background variation if present and allows each lawn to be isolated manually with cursors (Fig. 4c). It then converts the pixel intensities of the line scan at each time point to a standard deviation of intensity across each lawn. Resultant data are then curve fit within Igor Pro as a simple exponential decay from which a mean lifetime or half-life can be calculated for the granules intersected by the line. The graph in Fig. 4d is derived from the combined data from four lawns undergoing complete exocytosis in 10 mM Ca^{++}. Perturbation of the DIC image upon addition of Ca^{++} is seen as a "blip" which serves as a convenient marker of $t=0$. Typically, there is a variable lag period between addition of Ca^{++} and the initial decay in a given lawn. The assay shows that exocytosis is >90 % complete within 5 s after initiation.

Assuming an exponential decay for granule fusions in which the rate of loss of granules is proportional to the number remaining, we used the *exp_XOffset* fit function in IgorPro [$y_0+A\ \exp(x-x_o/\tau)$], where τ is the mean lifetime and x_0 the initial start of the decay. For the combined four lawns analyzed in Fig. 4d, $\tau=3.01\pm0.06$ s corresponding to a half-life (time for half of the granules to exocytose $t_{1/2}=\tau\ln2$) of 2.01 s. In addition, since data sampling rates in the line scan assay can be made very high, it is possible to obtain a large number of data points for the initial portions of the kinetic curves. This high sampling rate allows a more accurate estimate of initial rate of exocytosis to be derived. The initial rate was estimated for this curve by a linear fit of the first 500 ms as 25 %/s. This fitting function is also included in our Igor Pro subroutine.

Two-dimensional image analysis of exocytosis

The goal of our technique was to monitor the fusion progress over time, which required a technique for fast acquisition of pixel intensities. Thus, the line scan assay was ideal because it uses a small subset of the data from a field in order to acquire data rapidly. To obtain all the pixel data from an image of a given lawn, we also collected whole images for post-acquisition analysis with the image analysis package Volocity. Since DIC images were acquired on a confocal microscope, acquisition times were limited by the photomultiplier and scanning rates. We routinely acquired images with the 20X objective at ~3.5 Hz to obtain kinetic data from whole lawns. Combined, these two approaches gave us the temporal resolution necessary for kinetic analysis of cortical granule secretion.

In order to monitor fusion of cortical granules from an entire lawn, we imported a time series of images into Volocity and defined circular ROIs to fit individual lawns as shown in Fig. 5. Using the ROI functions *Measure* and *Threshold Measure Intensities*, pixel data were converted into a *Measurement* item and tabulated in a spreadsheet. Next, the intensity, standard deviation, and acquisition-time columns were imported into IGOR Pro for quantification, graphing of decay curves, and further analysis. The results from analysis of either line scans or two-dimensional images yielded essentially the same curves. For the lawn shown, triggered with 1 mM free Ca^{++}, the initial decay rate was 29 % and the exponential x-offset function curve fit yielded a mean lifetime $\tau=1{,}141\pm60$ ms with $t_{1/2}=791$ ms (Fig. 5).

An important advantage of two-dimensional analysis is that changes in morphology can be obtained at each time point for one or several lawns. Different responses of different regions of the lawn are easily analyzed by choice of ROI. This is illustrated in Fig. 6, in which lawns were triggered with 1 mM free Ca^{++}. Under these high Ca^{++} conditions, we consistently observed an "outside-in" pattern of fusion, which eventually

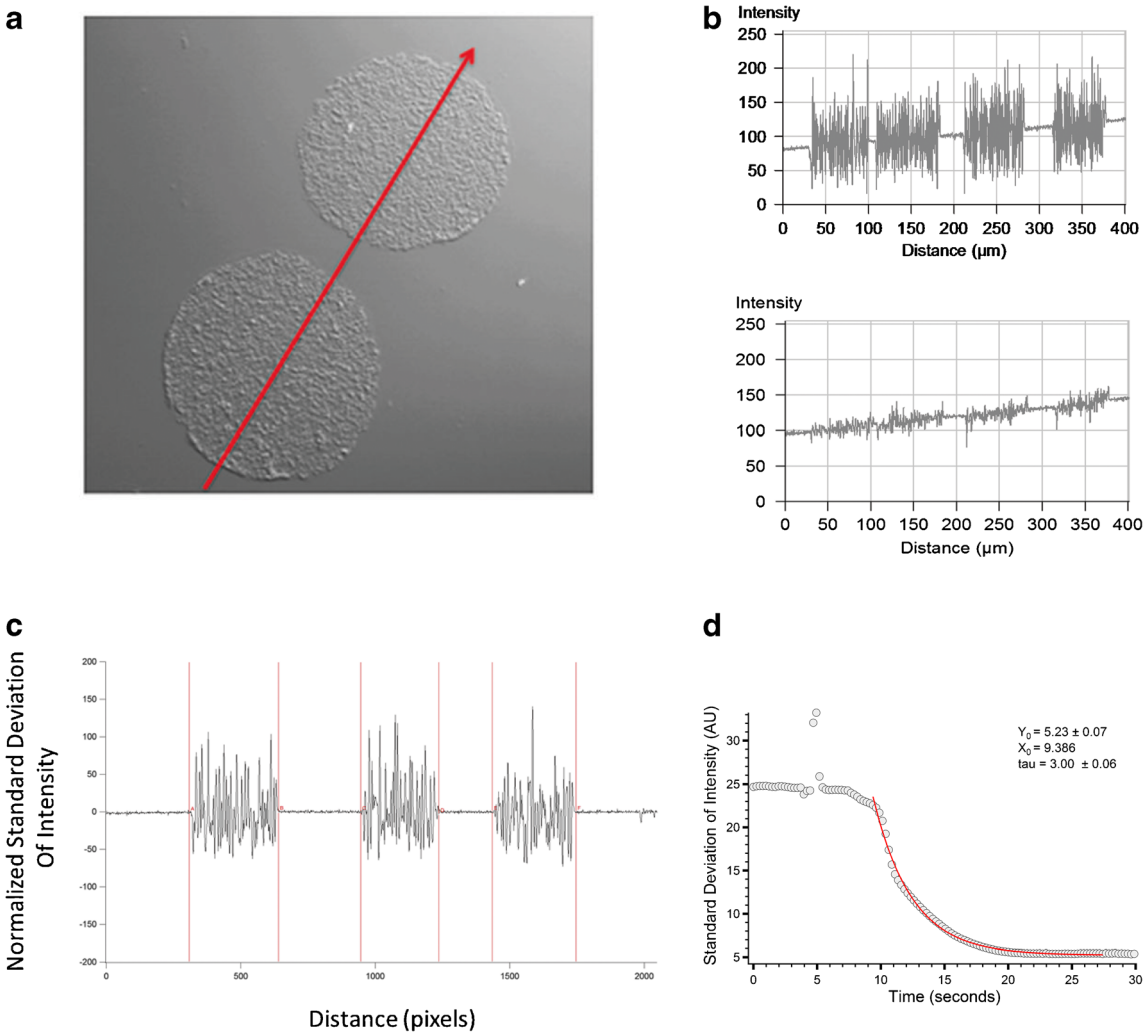

Fig. 4 Line scan assay. **a** Placement of a single-pixel wide line scan across two cortical lawns. **b** Intensity scans through both lawns in A before and 10 s after 10 mM Ca^{++}addition. **c** Representative line scans through three lawns before Ca^{++} addition after normalization of background with cursors set to isolate data from each lawn using the LS Analysis subroutine in Igor Pro. **d** Composite decay curve taken from four lawns shows loss of contrast with time during exocytosis measured as standard deviation of average pixel intensities, fit with an exponential function (*red line*)

led to complete exocytosis of the entire lawn's granules. Note that this phenomenon can also be detected by simulating line scans (using linear ROIs) through the center of lawns in 2D images in Volocity (insets).

A more detailed analysis of the image series from which Fig. 6 was drawn shows the exocytosis of a portion of the ~2,000 individual granules/lawn in the focal plane as a function of their position within the lawn (Fig. 7a). Linear ROIs of as few as 10–15 pixels within Volocity (Fig. 7b) show that individual granules undergo loss of contrast over essentially the same time interval no matter their position within a lawn (~500 ms), while the time of initiation for the individual exocytoses increases towards the center of the lawn.

In order to determine the spread of exocytosis from outside to inside, we plotted the decay kinetics from a series of ROIs shown in Fig. 8. These were formed by subtraction of concentric circular ROIs whose diameters were decreased by a constant value. This resulted in the nested concentric rings shown, and decay constants for the granule populations within each of the rings were compared with that from the entire lawn. The results provided a set of well-separated decay curves which differed in time of initiation and displayed similar but somewhat more complex decay curves moving towards the center of the lawn. The overall decay curve then is the sum of a set of similar but progressively slower decay curves beginning at different times. This apparent "wave" of exocytosis proceeds towards the center at a speed of ~5–10 μm/s. The initial decay rate of the outer ring was estimated at 71 %/s, whereas the initial rate for the entire lawn was only 29 % reflecting its heterogeneity. Fitting the outer ring of this lawn to an exponential x-offset function in Igor yielded a mean lifetime of 294±7.4 ms corresponding to a half-life for exocytosis in this region of $t_{1/2}$=203 ms. In contrast, the complex total decay curve yielded τ=1,141±60 ms with $t_{1/2}$=791 ms.

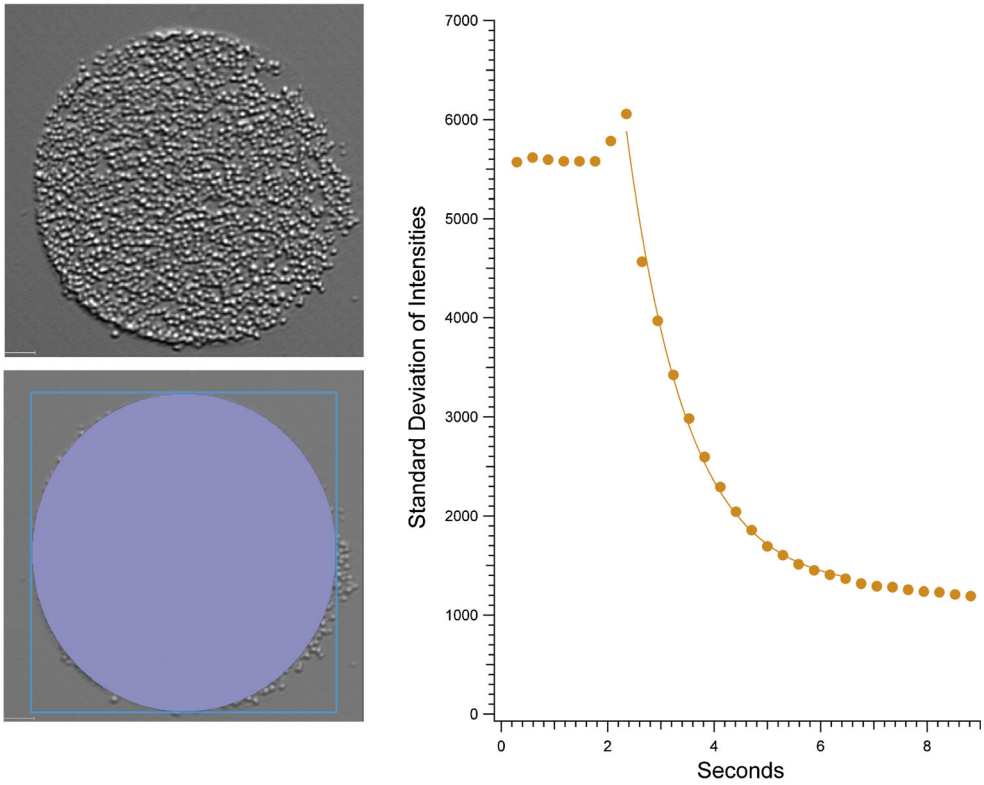

Fig. 5 Image analysis assay. An individual lawn was set as a region of interest (*ROI*; *blue*) and analyzed in Volocity to generate a decay curve of standard deviation of intensities versus time of image acquisition. The mean intensities for the series of images used to generate the standard deviation curve in Volocity were 24,000–25,000 AU

Ca^{++} sensitivity

The fraction of granules undergoing exocytosis at lower concentrations of free Ca^{++} can be obtained in endpoint assays from the difference between the beginning and ending levels of mean standard deviation for the pixel intensities. To derive the percent exocytosis, the resulting value is then normalized to an endpoint value for complete exocytosis for each preparation obtained after addition of excess Ca^{++} (10 mM). We have generated Ca^{++} sensitivity curves from endpoint data obtained by either line scan or image analysis. This analysis can be done with individual lawns, but it is also possible with a programmable motorized stage, to sample several regions each containing multiple lawns before and after addition of various concentrations of free Ca^{++} to provide high throughput averaged data for the entire population on the coverslip. Furthermore, since the background intensity between lawns does not change, it is not necessary to sample only pixels from individual lawn ROIs.

Figure 9 shows a Ca^{++} sensitivity curve constructed from three independent experiments. Data at each free Ca^{++} concentration was averaged from nine positions on the coverslip, each position containing ~50 lawns. When fit to a sigmoidal function, our data yielded a value of 50 % exocytosis at 16 μM Ca^{++} (the half maximal effective concentration or EC50) with

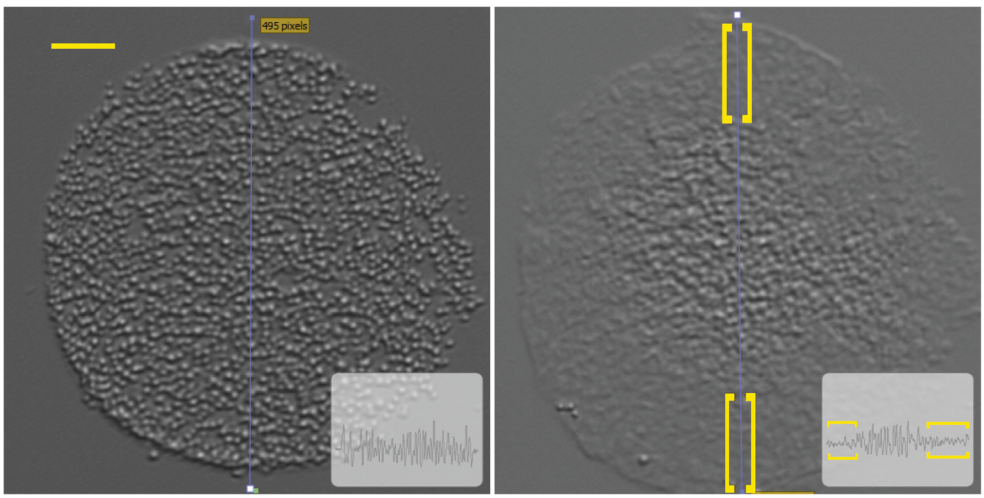

Fig. 6 Exocytosis from the periphery to interior of a lawn in high Ca^{++}. Two images taken before and during exocytosis (1.47 s after initiation). Linear regions of interest with pixel intensities vs. position plotted in the insets show the progression of exocytosis from periphery to interior. Note that peripheral regions (indicated in *yellow brackets*) show decreased contrast while the center is unchanged. *Yellow bar* = 10 μm

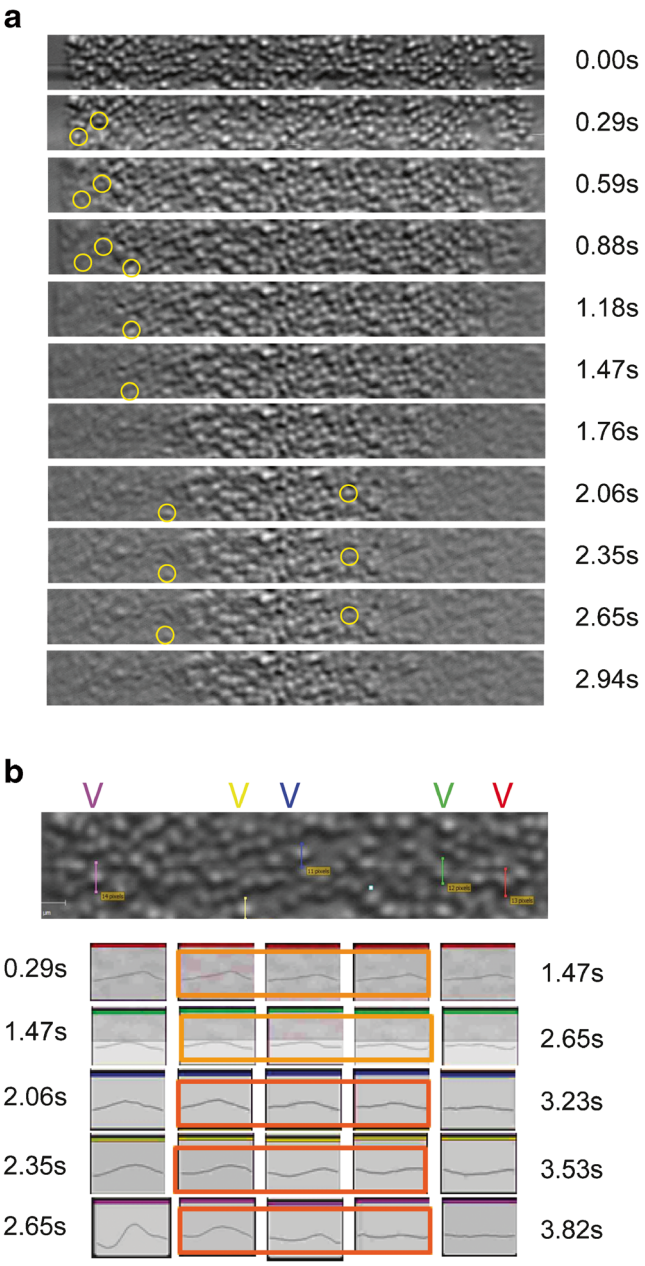

Fig. 7 Image analysis of individual exocytosis events. **a** A single ROI shown for successive images of the lawn in Fig. 6. Individual granules are circled as they each undergo exocytosis over a time span of ~500 ms. **b** *Upper panel* linear ROIs of 10–15 pixels were drawn across individual granules indicated before Ca^{++} addition. *Lower panels* the decay of intensity is plotted versus times indicated. The *upper bar* of each trace is color-coded to the granules indicated in the upper panel

exocytosis reaching >98 % by ~40 μM free Ca^{++}. The values of free Ca^{++} needed for >95 % exocytosis are referred to hereafter as the optimal Ca^{++} values.

In addition to providing Ca^{++} sensitivity curves, we were able to capture the spatial patterns of exocytosis as it progresses at suboptimal Ca^{++} concentrations. Regions of exocytosis appear to originate at several points in the lawn, expanding progressively, sometimes overlapping other regions, and then ceasing. Therefore, typical endpoint experiments show patches of exocytosis across the lawns rather than randomly distributed individual cortical granule events (Fig. 10). This suggests initiation from independent sites, propagation to adjacent granules, and possibly a self-limiting feedback mechanism.

Discussion

Methodology

We present a method using DIC microscopy to qualitatively and quantitatively monitor the progress of exocytosis of cortical granules (vesicles) in cortical lawn (planar) preparations from sea urchin eggs. It can be used to monitor fusion simultaneously from large numbers of lawns, individual lawns, or subregions of individual lawns. The procedure provides rapid data acquisition and generates kinetic and endpoint data comparable to previously published procedures, while also allowing simultaneous monitoring of morphological transitions and maintaining the spatial relationships of cellular components. We were able to derive kinetics of the entire course of exocytosis from which could be derived initial rates, percent exocytosis, and Ca^{++} sensitivity curves. These parameters are routinely used to study fusion or exocytosis in a variety of cortical granule assay systems such as planar lawns, cell surface complexes, or suspensions of purified granules ([3, 5, 24]). In addition, complex kinetic curves could be resolved into spatially discrete subcomponents.

Quantitative analysis of exocytosis of lawns has been achieved previously with light scattering microscopy in specially constructed flow chambers [11]. We chose to use open reaction vessels that are easily constructed and disposable. These vessels allow introduction and rapid exchange of solutions and are compatible with high-resolution differential interference contrast microscopy for quantitative monitoring. Commercial or lab-constructed flow units require advanced machining skills and may not allow sufficiently rapid solution mixing for analysis of exocytosis. Because they are expensive to fabricate, perfusion devices are reused multiple times and so must be reassembled for each run.

The open system used here on an inverted microscope permits rapid change in solvent conditions with continuous monitoring of alterations of lawn morphology. The rates of solvent mixing we achieved (~500 ms) are comparable to those reported using a specially constructed stop flow chamber (2,000 ms at low pressure and 500 ms at high pressure) [11].

Kinetics

The rate of solvent mixing in any in vitro system is a potential limitation for analysis of the initial kinetics of fusion. Typically, the initial decay curve is fit with a straight line over the first 450–500 ms to yield an initial rate. This has been reported

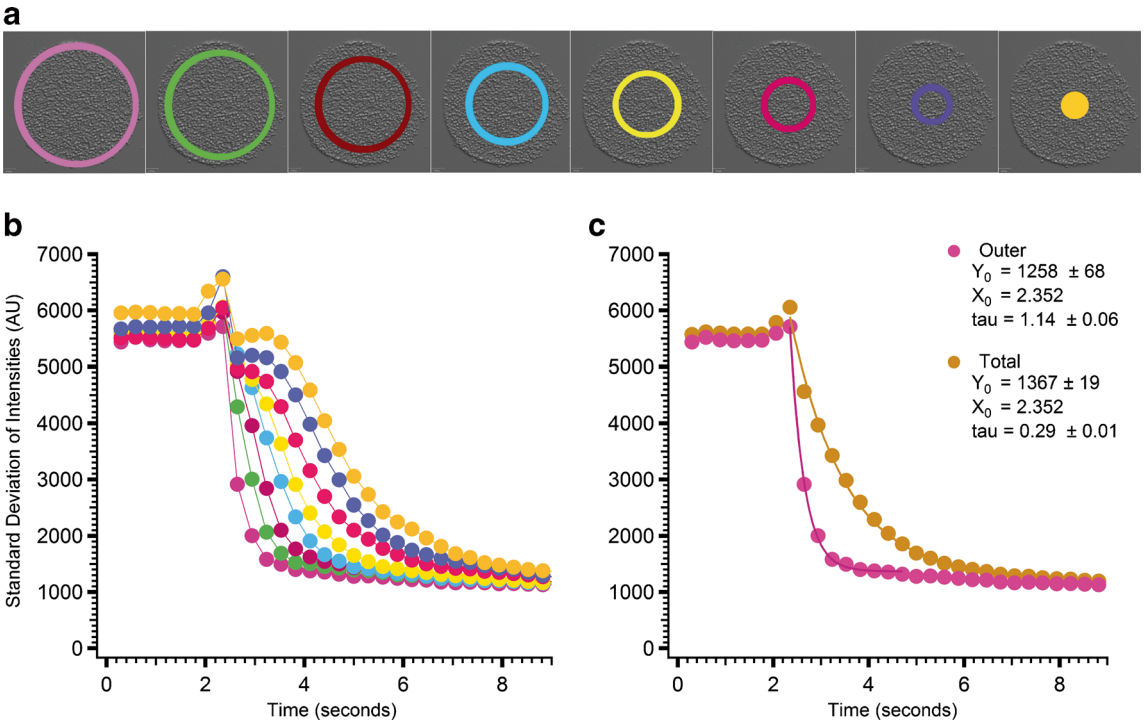

Fig. 8 Decay curves averaged within concentric ROI rings compared to composite data. **a** Concentric ring ROIs superimposed on an image of a lawn. **b** Color-coded decay curves initiated by 1 mM free Ca^{++} for each of the rings in **a**. The peripheral granules exocytose almost completely within 500–750 ms, whereas decay in the inner regions initiates progressively later with somewhat longer half-lives. **c** Composite curve for the entire lawn compared with the rapid decay of the outer ring, each fit with an exponential x-offset function

previously as 65 [3], 77 [5], and 74 % [16] at various free Ca^{++} concentrations above optimal. Our lawns yielded an initial decay rate of 71 %/s (for peripheral CGs by image analysis) which compares favorably to these previous estimates.

The basis of our assay was differential interference contrast microscopy. DIC has the advantage of providing optical contrast, particularly at membranes separating cell compartments, which is created by differences in indices of refraction and specimen thickness. The symmetry, in the manner in which the two polarized light beams pass through the boundary of a compartment, results in reciprocal contrast (dark on one side, light on the opposite). Additionally, compared to using condenser aperture reduction or phase contrast optics, DIC uses fully open apertures which provide higher resolution and a narrow depth of field that allows for optical sectioning, making it superior to phase contrast or darkfield microscopy.

DIC intensity data can be rapidly collected by line scans or 2D images in a non-scanning mode with an appropriately fast camera and can also be combined with fluorescence confocal images. Although the line scan assay offers very rapid

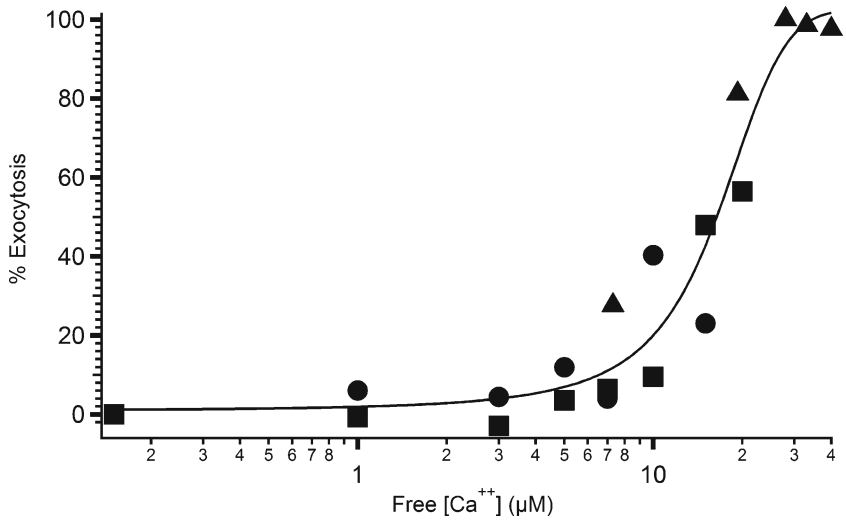

Fig. 9 Ca^{++} sensitivity curves. Endpoint data from 50 lawns were used to calculate the fraction of granules undergoing exocytosis at various free Ca^{++} concentrations. The semi-logarithmic plot was fit to a sigmoid function, which provides an EC_{50} of ~16 μM free Ca^{++}. Data from three experiments are indicated by different symbols. Concentration for >98 % exocytosis is 30–40 μM free Ca^{++}

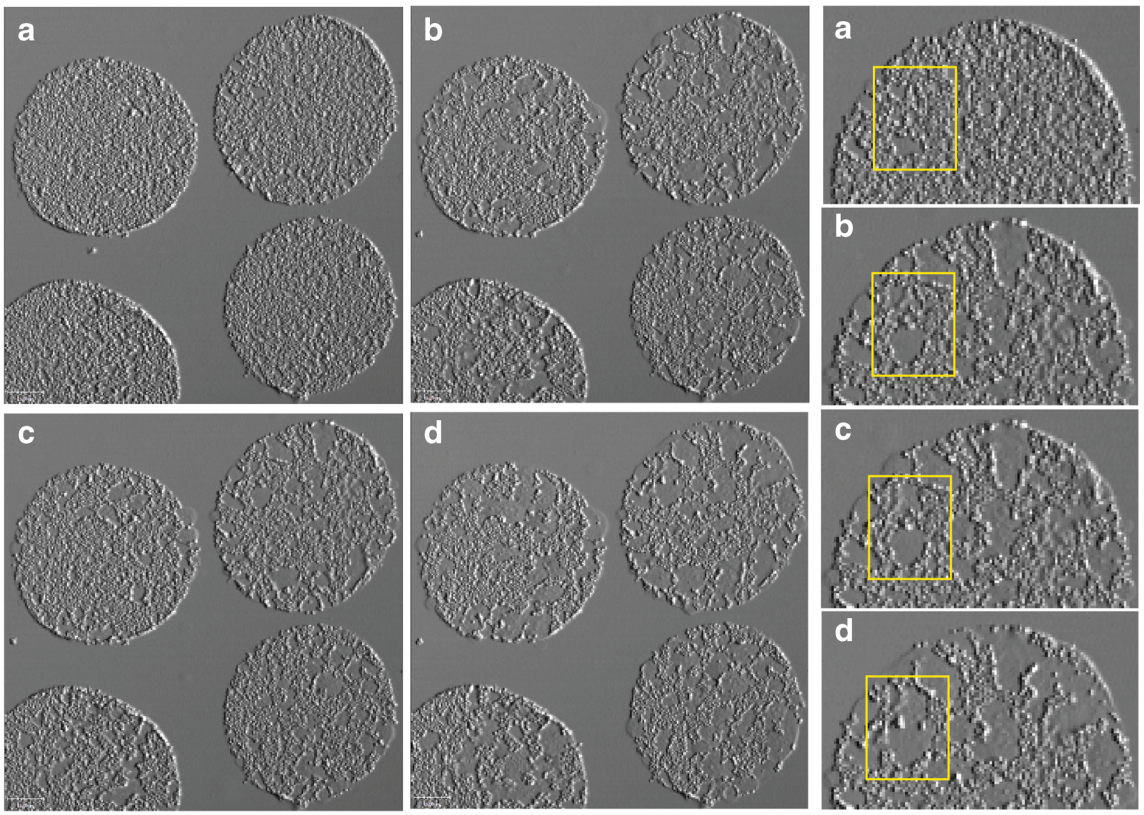

Fig. 10 Progression of exocytosis from several initiation points per lawn at suboptimal free Ca^{++} concentrations. Series of images of the same lawns at various times after 3 μM free Ca^{++} addition. During exocytosis at intermediate free Ca^{++} concentrations, decay rates are slower and exocytosis begins at several points, perhaps at single granules and radiates outward until ceasing, leaving "bare" patches of exocytosis surrounded by intact cortical granules. **a** 31.1 s, **b** 126.6 s, **c** 134.0 s, and **d** 154.1 s post-Ca^{++}. Magnified insets are shown in the right column

monitoring of exocytosis, one cannot follow visually the progression of exocytosis across an entire lawn. In addition, the line cannot be centered on each individual granule, and certain spatial information is lost. Detailed morphological changes in the preparation can only be obtained by comparison of before and after images. The use of a rapid acquisition digital camera (e.g., with a 30 Hz acquisition rate) can bypass the slower acquisition obtained from the scanning head of the confocal microscope which should make 2D data acquisition rates comparable with the line scan assay. Furthermore, either assay will allow monitoring local changes in Ca^{++} concentrations with Ca^{++} sensitive indicator dyes or membrane fusion or fluidity changes using FRET or FRAP techniques [28], all while maintaining the spatial relationships of the various cortical components.

Spatial aspects of cortical lawn exocytosis

Full exocytosis (and complete homotypic fusion of CGs) has been reported previously for free Ca^{++} concentrations generally exceeding 50 μM. Our values for Ca^{++} sensitivity are consistent with published data. We found optimal free [Ca^{++}] was ~40 μM with an EC50=16 μM. Although, occasionally, lower EC50s have been reported (4–5 μM for CSCs and CG/CG fusion [7, 8, 26] and 14 μM for planar lawns [2]), more typically values in the 20–50 μM range have been obtained (30 μM for lawns [26], 46 μM for CG/CG fusion [5, 6, 16]). The peak in vivo Ca^{++} transient in fertilized eggs of a different species of sea urchin (*Lytechinus pictus*) was estimated at 2.5–4.5 μM, and in the same paper, optimal free Ca^{++} for triggering isolated lawns was reported between 9 and 18 μM [17].

By following the progression of exocytosis with DIC microscopy, two heretofore unappreciated aspects of the in vitro pattern became apparent: one at suboptimal free Ca^{++} levels and one at excess Ca^{++}. Partial exocytosis or submaximal fusion of CGs has been previously reported at suboptimal concentrations of Ca^{++} [7, 25], but we are unaware of reports of the initiation of exocytosis from multiple points in each lawn which grow and then cease unless further Ca^{++} is added. Such data cannot be obtained from suspensions of CGs or even CSCs. Initiation of exocytosis by mechanical damage of lawns propagated to other lawns throughout the preparation was noted by Vacquier which he attributed to Ca^{++} originating in the damaged CGs themselves [24].

It is possible that the initiation effect is an artifact of inhomogeneities in adherence to the cover slip that make some regions offer less resistance to exocytosis. Another possible interpretation of the suboptimal free Ca^{++}-initiated patterns we

observed is that there are preferential sites of initiation and limited extents of propagation from those sites with cessation perhaps due to decline of the signal intensity. We know of no reason why the most sensitive CGs would be arranged in a pattern. Based on CG-CG fusion data, submaximal responses to Ca^{++} of individual granules has been attributed to differences in individual CG Ca^{++} sensitivity rather than due to inactivation of individual granules [2], and these could be the source of the initial signals. In vivo, the wave of Ca^{++}-triggered exocytosis always initiates from the region of fusion of sperm with egg. Since polyspermic eggs will show multiple sites of initiation of exocytosis, it is possible that the most sensitive CGs are randomly distributed and correspond to the sites we see in vitro. The self-limiting aspect of this phenomenon is under investigation but might involve re-sequestration of Ca^{++} by adjacent endoplasmic reticulum fragments in the lawns. The contribution of local fluctuations in free Ca^{++} potentially due to release from ER or CG stores is not known and will require monitoring these levels during the progress of exocytosis. Such spatial details of Ca^{++} flux will be amenable to quantitative analysis with this assay.

It is instructive to compare the pattern of exocytosis to what actually occurs in vivo. Using a clever assay to simultaneously monitor exocytosis by content mixing and surface membrane on live sea urchin eggs at fertilization, Terasaki was able to show that individual granules did not exocytose in order as might be expected from a wave of optimal Ca^{++}, but appeared to fuse in irregular spatial patterns [19]. Content mixing occurred over 0.1–0.2 s in *Lytechinus variegatus*. In addition, exocytosis was not strongly correlated with local Ca^{++} increases assayed by the Ca^{++} indicator Calcium Green Dextran. There was also a substantial lag period (of almost 8 s) after maximal Ca^{++} levels were reached before exocytosis was detected, which suggests rate-limiting events downstream of the Ca^{++} sensing mechanism. The lag period may relate to the variable lag periods we see in vitro between addition of Ca^{++} and exocytosis in vitro. Ca^{++} sensing is likely to depend on synaptotagmin which is found on the granules [14]. Although exocytosis typically occurs from the point of sperm entry around the surface of the egg over 1–2 min, the random nature of exocytosis over limited regions and the lack of a tight correlation of $[Ca^{++}]$ and exocytosis suggested that a simple model of Ca^{++} triggering of a uniform set of granules is incorrect. Unlike our results at suboptimal Ca^{++} concentrations, however, there did not appear to be spreading of exocytosis events from a few focal points to adjacent granules. The basis of this phenomenon is currently under investigation.

In contrast with the data on suboptimal Ca^{++}, exocytosis appeared to proceed uniformly in a peripheral to central direction in lawns exposed to large excesses of free Ca^{++}. As noted above, we were able to calculate an initial rate of exocytosis at the periphery that was similar to the maximal initial rates reported in the literature. However, initial rates appear to decline somewhat with locations closer to the center of the lawn. This unusual "outside-in" relationship seen at high Ca^{++} concentrations indicates that the overall decay rate in the lawn reflects a sum of initiations that begin at the periphery and progress towards the center. Despite this phenomenon, individual CGs appear to undergo exocytosis over a similar time interval regardless of their location; once fusion is initiated, it appears to proceed by a similar mechanism. Therefore, overall kinetics for this progression are similar to those obtained in other assays but are apparently the resultant sum of a series of fusions whose initiations proceed at a fairly constant rate towards the center. This behavior is not consistent with a random arrangement of more sensitive CGs. Whether it arises as an artifact of nonuniform adhesion of lawns that allows for a "lifting" effect of the fused membrane that facilitates further fusion, or whether it has a physiologically relevant foundation such as mutual inhibition feedback loops, is under investigation. In any event, the phenomenon illustrates the ability of our assay to quantify spatial inhomogeneities in exocytosis responses.

In conclusion, our assay system appears to include a number of phenomena that may be related to the in vivo behavior of CGs and that are not accessible in CSC or CG suspensions. The system will allow for precise manipulation of the environment of the granules, evaluation of local free Ca^{++} concentrations with concomitant exocytosis, estimation of ER and CG contributions to the Ca^{++} fluxes, manipulation of protein and lipid composition, and quantification of overall kinetics from large numbers of lawns in the context of a minimally disturbed cortical structure.

Acknowledgments We gratefully acknowledge Julie Fitzgerald and Fadi Hamati for technical assistance, Patrick Williamson for helpful discussions, and Ron Hebert for reaction vessel construction. Support was received from a SOMAS-URM grant through the Howard Hughes Medical Institute (grant no. 52005120) and the National Science Foundation (grant no. DUE-0930153) to J.G.T. and a Faculty Research Award of the Axel Schupf'57 Fund for Intellectual Life to D.P.

References

1. Avery J, Ellis DJ, Lang T, Holroyd P, Riedel D, Henderson RM, Edwardson JM, Jahn R (2000) A cell-free system for regulated exocytosis in PC12 cells. J Cell Biol 148:317–324
2. Blank PS, Cho MS, Vogel SS, Kaplan D, Kang A, Malley J, Zimmerberg J (1998) Submaximal responses in calcium-triggered exocytosis are explained by differences in the calcium sensitivity of individual secretory vesicles. J Gen Physiol 112:559–567
3. Blank PS, Vogel SS, Malley JD, Zimmerberg J (2001) A kinetic analysis of calcium-triggered exocytosis. J Gen Physiol 118:145–156
4. Chen X, Arac D, Wang T, Gilpin CJ, Zimmerberg J (2006) SNARE-mediated lipid mixing depends on the physical state of the vesicles. Biophys J 90:2062–2074
5. Churchward M, Rogasevskaia T, Hofgen J, Bau J, Coorssen J (2005) Cholesterol facilitates the native mechanism of Ca2+-triggered membrane fusion. J Cell Sci 118:4833–4848

6. Churchward MA, Rogasevskaia T, Brandman DM, Khosravani H, Nava P, Atkinson JK, Coorssen JR (2008) Specific lipids supply critical negative spontaneous curvature—an essential component of native Ca^{2+}-triggered membrane fusion. Biophys J 94:3976–3986
7. Coorssen JR, Blank PS, Tahara M, Zimmerberg J (1998) Biochemical and functional studies of cortical vesicle fusion: the SNARE complex and Ca^{2+} sensitivity. J Cell Biol 143:1845–1857
8. Coorssen JR, Blank PS, Albertorio F, Bezrukov L, Kolosova I, Chen X, Backlund PS Jr, Zimmerberg J (2003) Regulated secretion: SNARE density, vesicle fusion, and calcium dependence. J Cell Sci 116:2087–2097
9. Decker SJ, Kinsey WH (1983) Characterization of cortical secretory vesicles from the sea urchin egg. Dev Biol 96:37–45
10. Detering NK, Decker GL, Schmell ED, Lennarz WJ (1977) Isolation and characterization of plasma membrane-associated cortical granules from sea urchin eggs. J Cell Biol 75:899–914
11. Kaplan D, Bungay P, Sullivan J, Zimmerberg J (1996) A rapid flow perfusion chamber for high-resolution microscopy. J Microsc 181: 286–297
12. Kinsey WH, Decker GL, Lennarz WJ (1980) Isolation and partial characterization of the plasma membrane of the sea urchin egg. J Cell Biol 87:248–254
13. Kopf GS, Moy GW, Vacquier VD (1982) Isolation and characterization of sea urchin egg cortical granules. J Cell Biol 95:924–932
14. Leguia M, Wessel GM (2007) The many faces of egg activation at fertilization. Signal Transduct 7:118–141
15. Raveh A, Valitsky M, Shani L, Coorssen JR, Blank PS, Zimmerberg J, Rahamimoff R (2012) Observations of calcium dynamics in cortical secretory vesicles. Cell Calcium 52:217–225
16. Rogasevskaia TP, Coorssen JR (2011) A new approach to the molecular analysis of docking, priming, and regulated membrane fusion. J Chem Biol 4:117–36
17. Steinhardt R, Zucker R, Schatten G (1977) Intracellular calcium release at fertilization in the sea urchin egg. Dev Biol 58:185–196
18. Sudhof TC (2004) The synaptic vesicle cycle. Annu Rev Neurosci 27:509–547
19. Terasaki M (1995) Visualization of exocytosis during sea urchin egg fertilization using confocal microscopy. J Cell Sci 108:2293–2300
20. Terasaki M, Henson J, Begg D, Kaminer B, Sardet C (1991) Characterization of sea urchin egg endoplasmic reticulum in cortical preparations. Dev Biol 148:398–401
21. Terasaki M, Reese TS (1992) Characterization of endoplasmic reticulum by co-localization of BiP and dicarbocyanine dyes. J Cell Sci 101:315–322
22. Terasaki M, Sardet C (1991) Demonstration of calcium uptake and release by sea urchin egg cortical endoplasmic reticulum. J Cell Biol 115:1031–1037
23. Trikash IO, Kolchinskaya LI (2006) Fusion of synaptic vesicles and plasma membrane in the presence of synaptosomal soluble proteins. Neurochem Int 49:270–285
24. Vacquier VD (1975) The isolation of intact cortical garanules from sea urchin eggs: calcium ions trigger granule discharge. Dev Biol 43: 62–74
25. Vogel SS, Blank PS, Zimmerberg J (1996) Poisson-distributed active fusion complexes underlie the control of the rate and extent of exocytosis by calcium. J Cell Biol 134:329–338
26. Vogel SS, Zimmerberg J (1992) Proteins on exocytic vesicles mediate calcium-triggered fusion. Proc Natl Acad Sci 89:4749–4753
27. Wojcik SM, Brose N (2007) Regulation of membrane fusion in synaptic excitation-secretion coupling: speed and accuracy matter. Neuron 55:11–24
28. Wong JL, Wessel GM (2008) FRAP analysis of secretory granule lipids and proteins in the sea urchin egg. Methods Mol Biol 440: 61–76
29. Zimmerberg J, Sardet C, Epel D (1985) Exocytosis of sea urchin egg cortical vesicles in vitro is retarded by hyperosmotic sucrose: kinetics of fusion monitored by quantitative light-scattering microscopy. J Cell Biol 101:2398–2410